Direct Observation of Graphene Growth and Associated Copper Substrate Dynamics by *in Situ* Scanning Electron Microscopy

Zhu-Jun Wang,[†] Gisela Weinberg,[†] Qiang Zhang,[†,⊥] Thomas Lunkenbein,[†] Achim Klein-Hoffmann,[†] Michalina Kurnatowska,[‡] Milivoj Plodinec,[§] Qing Li,[∥] Lifeng Chi,[∥] R. Schloegl,[†] and Marc-Georg Willinger*[,†]

[†]Fritz Haber Institute of the Max Planck Society, D-14195 Berlin-Dahlem, Germany, [‡]Institute of Low Temperature and Structure Research, Polish Academy of Sciences, 52-422 Wroclaw, Poland, [§]Laboratory for Molecular Physics, Ruđer Bošković Institute, 10000 Zagreb, Croatia, and [∥]Institute of Functional Nano & Soft Materials (FUNSOM), Collaborative Innovation Center of Suzhou Nano Science and Technology, Soochow University, Suzhou 215123, Jiangsu, China. [⊥]Present address: Beijing Key Laboratory of Green Chemical Reaction Engineering and Technology, Department of Chemical Engineering, Tsinghua University, Beijing 100084, People's Republic of China.

ABSTRACT This work highlights the importance of *in situ* experiments for an improved understanding of graphene growth on copper *via* metal-catalyzed chemical vapor deposition (CVD). Graphene growth inside the chamber of a modified environmental scanning electron microscope under relevant low-pressure CVD conditions allows visualizing structural dynamics of the active catalyst simultaneously with graphene nucleation and growth in an unparalleled way. It enables the observation of a complete CVD process from substrate annealing through graphene nucleation and growth and, finally, substrate cooling in real time and nanometer-scale resolution without the need of sample transfer. A strong dependence of surface dynamics such as sublimation and surface premelting on grain orientation is demonstrated, and the influence of substrate dynamics on graphene nucleation and growth is presented. Insights on the growth mechanism are provided by a simultaneous observation of the growth front propagation and nucleation rate. Furthermore, the role of trace amounts of oxygen during growth is discussed and related to graphene-induced surface reconstructions during cooling. Above all, this work demonstrates the potential of the method for *in situ* studies of surface dynamics on active metal catalysts.

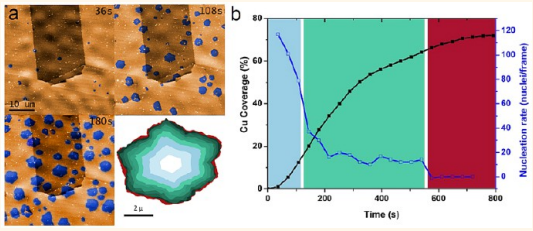

KEYWORDS: *in situ* · graphene growth · electron microscopy · catalysis

The breakthrough of graphene-based technology depends on the ability to produce high-quality graphene sheets on an industrial scale.[1] Among the various strategies currently followed,[2−7] the catalytic chemical vapor deposition (CVD) process on polycrystalline copper foils has demonstrated potential for a cost-effective, controllable synthesis of few- or single-layer graphene.[2] So far, alterations and improvements of growth conditions have led to various morphologies of graphene domains[8−12] and successful growth of graphene single crystals up to several millimeters.[9,13] To date, the optimization of process conditions on the basis of feedback from *ex situ* characterization of the product is still very much state of the art. However, growth models that rely on *ex situ* observations are in principle incapable of providing a complete picture of the dynamics of a CVD process. As a consequence, the understanding of the CVD growth dynamics on copper remains limited and empirical. Indeed, many assumptions about the growth mechanisms that were postulated from *ex situ* studies await confirmation by direct observation.

From heterogeneous catalysis we learn that a mechanistic insight can only be obtained on the basis of *in situ* techniques that are capable of capturing the interaction of a catalyst with the gas phase while the product is formed.[14−16] The value of *in situ* studies in deducing details of graphene growth either through CVD growth or *via*

* Address correspondence to willinger@fhi-berlin.mpg.de.

Received for review October 20, 2014 and accepted January 13, 2015.

Published online January 13, 2015
10.1021/nn5059826

precipitation from the bulk was documented for a number of transition metal substrates such as Ni, Ru, Rh, and Ir using low-energy electron microscopy (LEEM),[17−20] photoemission electron microscopy (PEEM),[21] scanning tunneling microscopy (STM),[22,23] and near ambient pressure X-ray photoelectron spectroscopy (NAP-XPS).[24] However, due to the low dehydrogenation activity of copper and the required high temperature, only spatially integrated spectroscopic data are available from *in situ* XPS and X-ray diffraction (XRD) on polycrystalline films under LP-CVD growth conditions.[25] Surface imaging during graphene growth on copper has so far been realized only under ultrahigh vacuum (UHV) conditions using LEEM and the deposition of elemental carbon[26,27] and by *in situ* SEM on graphene growth on Ni *via* segregation of bulk dissolved carbon.[28] To date, there is no visual and spatially resolved information available regarding the state of the surface and details of graphene growth dynamics on copper under relevant catalytic CVD conditions.

As a consequence, temperature-, pressure-, and atmosphere-related substrate dynamics and their effect on graphene nucleation and growth are still unclear.

Here we show that *in situ* observation under conditions of cold wall, low-pressure (LP)-CVD is possible by utilizing a modified environmental scanning electron microscope (ESEM) (see Supporting Information).

Using this instrument, we are able to follow a complete CVD cycle from substrate annealing to graphene growth and subsequent cooling. Hence, we obtain a complete and undisturbed picture of the involved dynamics without the need for sample transfer. The latter is important for the validation of mechanistic models that are derived on the basis of postgrowth observation, *i.e.*, under the premise that sample transfer and changes in temperature and atmosphere do not induce relevant modifications of the graphene−substrate interaction.[29,30]

In the ESEM, visualization of graphene growth is enabled by the high sensitivity of the secondary electron (SE) signal to changes in the work function, the low cross section of graphene for secondary electron generation, and the attenuation of secondary electrons emitted from the Cu substrate by the covering graphene layer.[31−33]

Since the investigations are made inside a microscope, a simultaneous observation of graphene as the reaction product and associated morphological changes of the catalyst is possible over a large range of magnifications. Detailed nanometer-scale information can therefore easily be embedded in a global picture that is obtained at low magnifications. The *in situ* experiments presented here reveal the dynamic nature of the process in an unparalleled way and provide important insights on the growth kinetics and the substrate−film interactions at the micro- to nanometer scale. Furthermore, it is one of the few cases in catalysis where the dynamics of a working catalyst can be observed while, at the same time, the product of the reaction can directly be seen.

RESULTS

In the following, we present observations made during several complete processes of graphene growth *via* metal-catalyzed LP-CVD inside the chamber of an ESEM. Each of the experiments involved substrate annealing, graphene nucleation and growth, and, finally, substrate cooling. In the second part of the paper, the observations are analyzed, discussed, and related to findings of postgrowth studies that are reported in the literature.

Copper Annealing. All samples were annealed at 1000 °C under a hydrogen flow of 8 sccm at a pressure of 4.4×10^{-2} Pa for 50 min inside the ESEM chamber. The initial polycrystalline copper foil shows a homogeneous contrast in the SE image (Figure 1a). With increasing temperature, small changes in contrast indicate desorption of adsorbed surface species and removal of contaminants from the Cu surface. Above 380 °C, the onset of morphological changes on the surface of the Cu foil can be observed. Surface reconstructions lead to the appearance of a pronounced electron-channeling contrast pattern due to differently oriented crystalline grains as shown in Figure 1b and the SI Movie M1. Above 400 °C, the temperature is high enough for abnormal grain growth and migration, causing expansion of grains that expose low-energy faces (mainly ⟨100⟩, ⟨110⟩, and ⟨111⟩)[34] at the expense of energetically less favorable ones. As a consequence of surface reconstruction, processing-induced artifacts from foil rolling start to disappear. Above 600 °C, contrast changes indicate desorption of remaining carbonaceous deposits. With rising temperature, the grain size of the polycrystalline foil further increases. At around 800 °C (Figure 1c) small particles of bright contrast start appearing at the surface. They measure around 10−200 nm in diameter and are mostly due to segregation of silicon contamination from the bulk to the surface (see Figure SI 1). Similar particles were reported by others and can frequently be observed in postgrowth SEM images in the literature.[2,8−11,29,30,35,36] Above 850 °C, these particles become mobile and start drifting across the surface in more or less random directions. Their drifting speed increases with temperature and is in the range 10−50 nm/s at 1000 °C (see SI Movie M1). The movement in random directions indicates an increased mobility of the copper surface and the onset of surface premelting.[37,38] As a consequence, remaining features due to foil production and signs of a crystalline surface such as steps and grain faceting disappear. However, due to contributions from electron channeling to

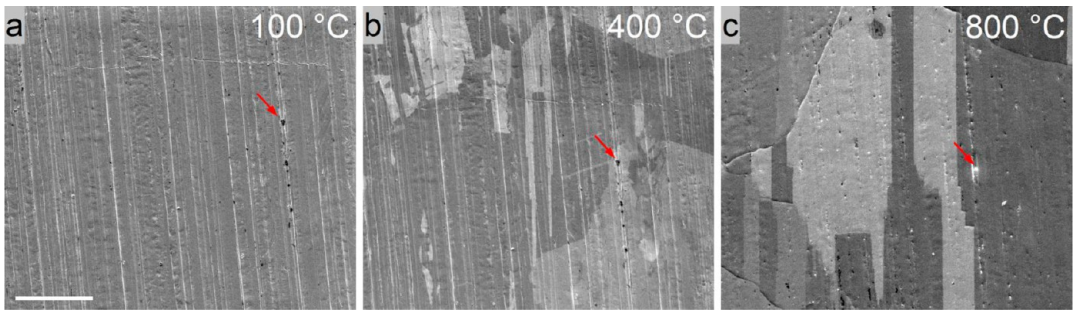

Figure 1. Surface modifications can be seen in snapshots taken during an annealing process at 100 °C (a), 400 °C (b), and 800 °C (c), respectively. A complete annealing process is shown in SI Movie M1. Red arrows reference identical positions on the foil. Sample movement is due to thermal drift. The scale bar measures 20 μm.

contrast in the secondary electron image, different orientations of grains below the premelted surface can still be detected.

Graphene Nucleation and Growth. Typically after annealing for 50 min at 1000 °C, the hydrogen flow was reduced to 4 and 0.1 sccm of C_2H_4 was added. The introduction of C_2H_4 can be detected as a change in SE image contrast and a slight increase of the chamber pressure and further confirmed with a mass spectrometer that is attached to the microscope. Formation of carbon deposits can generally be observed after an induction period of around 10 min, when spots of darker contrast start to appear on the surface of the copper film. A series of SEM images capturing the appearance and growth of carbon sheets on Cu at 1000 °C is presented in Figure 2 (and Si Movie M2). Although the resolution of the ESEM is not sufficient to detect the actual nucleation event, new flakes can be observed as soon as they reach a size of around 3 nm.

As a result of the high temperature and the substantial loss of copper due to sublimation,[39] the topography of the surface changes with growth time. Graphene-covered regions start to show up as hills between valleys of uncovered copper (see Figure SI 2).

With time, the growth speed of graphene flakes decreases until, finally, growth terminates, although ethylene and hydrogen are delivered at constant rate and the temperature remains constant. In agreement with earlier reports on LP-CVD, growth termination occurs regardless of the fact that the copper surface is not completely covered by graphene.[29,30]

Substrate Cooling. After termination of the growth process, the temperature of the substrate was decreased at a rate of 20 °C per min, while the flow of hydrogen and ethylene was kept constant. Snapshots taken during cooling are displayed in Figure 3 and provided as SI Movie M3. During cooling inside the ESEM, a copper surface reconstruction and the evolution of surface faceting are observed in the temperature range between 750 and 520 °C. Remarkably, the reconstruction underneath the carbon sheets is distinct and can easily be differentiated from the reconstruction of uncovered copper.

Characterization. After growth and cooling, the microscope was set to high-vacuum mode for optimized imaging conditions and postgrowth structural investigation. The as-grown sheets were furthermore characterized by Raman, AFM, STM, and TEM. On the basis of the Raman spectra and STM data, the grown sheets can be identified as high-quality single-layer graphene[40−42] (see Figure SI 3).

DISCUSSION

Graphene Growth Behavior. The nucleation and growth behavior can directly be extracted from the *in-situ*-recorded image sequences. Figure 4a shows the percentage of the graphene-covered copper surface area together with the change of the nucleation rate with time. Here, the nucleation rate is defined as the number of new graphene flakes that are detected per each recorded image frame. Values have been abstracted from an area measuring 9000 μm^2, in which a total of 507 nucleation events were registered (see Figure SI 2). The observed induction period and subsequent nucleation behavior strongly indicate an initial building up of carbon growth species on the substrate surface until supersaturation is reached and nucleation is initiated. The behavior is therefore similar to what was found by *in situ* LEEM[19] in the case of graphene growth on Ru and Ir. However, this is the first direct observation of an induction period in the case of CVD growth on copper. It confirms previous findings that were obtained *ex situ* on the basis of time-dependent growth studies.[10,30] With the ESEM data it is now possible to relate the nucleation behavior to the evolution of growth. During the initial phase (region I in Figure 4a), the radial growth of graphene sheets is roughly constant (central region in Figure 4b), hence, the square function-like onset of the integrated areal growth curve. The consumption of carbon building blocks due to nucleation and growth quickly leads to desaturation, which explains the drop in nucleation rate in the transition to the second growth phase (region II in Figure 4a). The fact that supersaturation cannot be upheld demonstrates that, under the chosen experimental conditions, the production rate

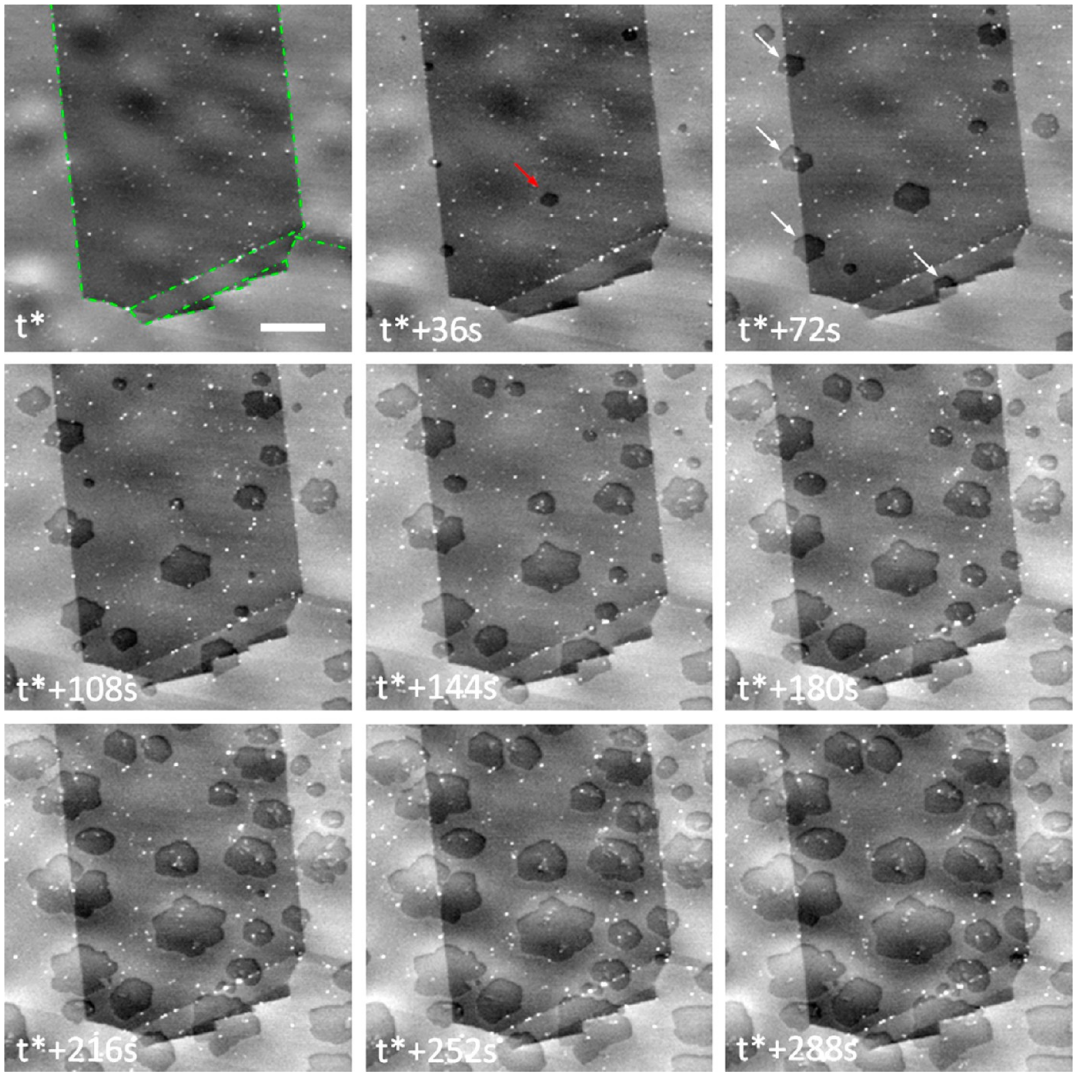

Figure 2. *In situ* **SEM images recorded at 1000 °C during LP-CVD growth showing the nucleation and growth of carbon sheets (characterized by darker contrast). White arrows highlight nucleation events at grain boundaries. t* corresponds to the induction period from C_2H_4 dosing until the first nucleation events can be detected. Growing graphene sheets are characterized by a dark contrast. Smooth contrast of the copper surface is due to a sublimation-induced surface buckling. Grain boundaries in the copper foil are highlighted by green dotted lines in the top left image. Differences in contrast for different grains are due to electron channeling. The scale bar measures 5 μm.**

of carbon growth species by catalyzed ethylene decomposition is lower than their total rate of consumption, either in nucleation and growth, or by recombination and desorption from the surface.

As a result of the shortage in building blocks, the growth mode changes from attachment-limited to surface-diffusion-limited growth.[8] Some of the observed sheets reflect this change in growth mode by a slight change in the growth shape (Figure 4b, in the transition from the first to the second phase). The accumulation of defects and partial etching of defective carbon from growing flakes by hydrogen[9] as well as differences in growth mechanisms at corners *versus* edges furthermore play a role in the shape transformation and the change of the growth front from a straight line to a corrugated pattern (Figure 4b).[43,44]

Although the nucleation rate drops significantly after the initial growth phase, some nucleation events are still observed during the second phase. Delayed nucleation events can be related to local inhomogeneity on the copper surface and variations in the time needed to reach the required supersaturation. As shown in Figure 4c, sheets nucleating at a later time show a similar initial growth behavior to early ones.

Direct observation of individual sheets reveals that the growth speed decreases faster when growth fronts of neighboring sheets approach each other. Indeed, it was found that, under the chosen experimental conditions, growing sheets generally do not merge, even if they nucleate close to one another (Figure 4d and Figure 5). The effect of the distance and location of neighboring graphene sheets on the growth front propagation is exemplified for different configurations

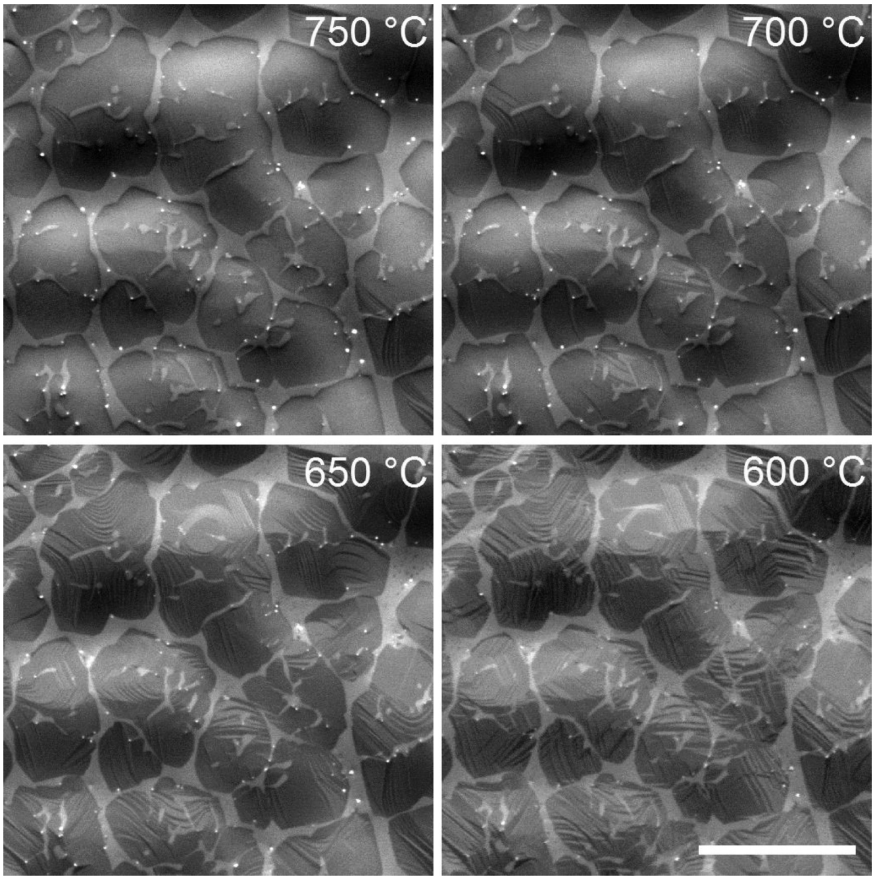

Figure 3. *In situ* **SEM images recorded during cooling, showing distinct morphological changes of the Cu surface underneath carbon sheets during cooling. The scale bar measures 10 μm.**

of neighbors in Figure 5a–d and f. The obvious mutual influence between growing sheets is indicative of the existence of a capture zone at the growth front. The capture zone is characterized by the lifetime of carbon growth species and their associated diffusion length on the copper surface.

Growth of individual sheets after nucleation in a locally supersaturated environment can therefore be described as follows. During the first phase, in which the radial growth rate is approximately constant, a newly formed nucleus grows in attachment-limited mode while building up a depletion zone at the growth front. Once this depletion zone has grown to its full size, which is determined by the diffusion length of growth species, the second phase of growth is entered. In this phase, growth is limited by capturing of growth species that diffuse through the diffusion layer and those that are produced by catalytic decomposition within the diffusion layer. Hence, growth follows a typical 2D film growth behavior.[45,46] Similarly to the Cu surface dynamics, the diffusion length of growth species depends on growth conditions and substrate grain orientation. Furthermore, depending on the degree of surface premelting, the grain orientation can influence the growth shape through anisotropic surface diffusion.[47] The third phase of growth is reached once the capture/diffusion zones of neighboring sheets start to overlap. Under the present growth conditions, this happens when the distance between growth fronts gets below about 3 μm. Growth at the corresponding growth fronts diminishes until balance is reached between carbon attachment and etching. A scheme of the discussed phases of graphene growth is shown in Figure SI 4.

This description of LP-CVD growth has several consequences for models derived on the basis of *ex-situ*-determined growth curves and will help to refine existing growth models.[48] First, there is not only one nucleation phase right after the induction period, which is followed by a phase of growth. Instead, substrate inhomogeneity combined with the limited diffusion length of carbon species can result in delayed nucleation events. Due to this, an integrated growth curve corresponds to a superposition of many individual growth curves starting at different times (see Figure 4c and Figure 5f). Second, the growth shape of individual sheets is influenced not only by surface dynamics and diffusion processes on a substrate grain but also by capture zones of nearby growing sheets, such as demonstrated in Figure 5f. Overall, the availability of growth species at the growth front determines which of the three described phases dominates

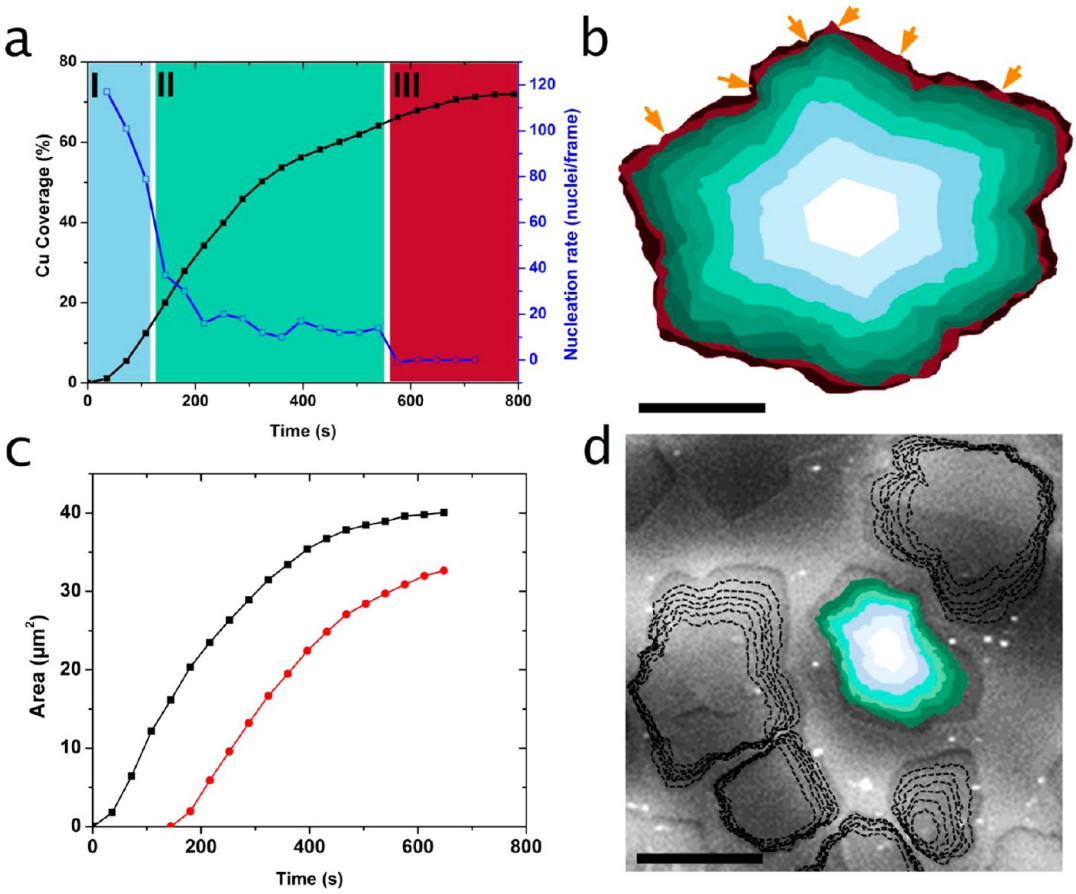

Figure 4. (a) Plot showing the increase of the graphene-covered Cu surface area with time (black curve). The nucleation rate (blue curve) is given as the number of new graphene flakes observed per recorded image frame during *in situ* ESEM imaging. The analyzed region is shown in Figure SI 2. (b) Superposition capturing the areal growth of a single flake (the one that is marked by a red arrow in Figure 2). Arrowheads indicate some places where etching is evident (see also Figure SI 5). (c) Areal growth of two flakes that appeared at different times (the black curve corresponds to the flake shown in (b); the red curve was abstracted from the colored sheet in (d)). (d) Shape evolution of neighboring graphene flakes in a superposition of seven image frames. The interval between subsequent image frames in (b) and (d) was 36 s. The scale bars in (b) and (d) measure 2 and 5 μm, respectively.

growth. Growth models should therefore be built on the basis of individual sheets under consideration of their local surrounding. Furthermore, crosstalk over extended distances can happen through the atmosphere. Differences in the gas phase and boundary layer chemistry could have an effect on the growth process on neighboring copper grains and thus influence the local kinetics of growth. It might therefore be of interest to study growth on single crystals.

The above description of growth is in accordance with previous results that showed that an extension of the linear growth regime is possible through an increase of the hydrocarbon partial pressure.[13] It results in a higher production rate of growth species, which delays the building up of a fully developed depletion zone at the growth front. Consequently, at sufficiently high hydrocarbon pressure, even complete copper coverage can be achieved.[49] Alternatively, the choice of a hydrocarbon source that shows a higher decomposition rate can lead to higher surface coverage under otherwise similar conditions.[25]

Direct observation of the growth front propagation further reveals the competition between graphene etching and growth at the beginning of phase three. Due to the reduced availability of growth species, carbon attachment can locally (*i.e.*, at defective regions) no longer counterbalance the etching (see arrowheads in Figures 4b and SI 5). However, growth can proceed after etching (Figure SI 5), indicating a possible repair mechanism for defect-free growth. This detail, which is missed in postgrowth observation,[13] probably plays an important role in the production of large, defect-free graphene sheets. Considering the many possible forms of carbon bonds, it is indeed possible that selective etching during growth controls the formation of two-dimensional graphene *versus* alternative three-dimensional forms of carbon, such as soot.

Cu Surface Dynamics. *In situ* ESEM experiments reveal substrate morphological changes during annealing and pronounced surface dynamics under conditions of growth. Under LP-CVD growth at 1000 °C, the loss of

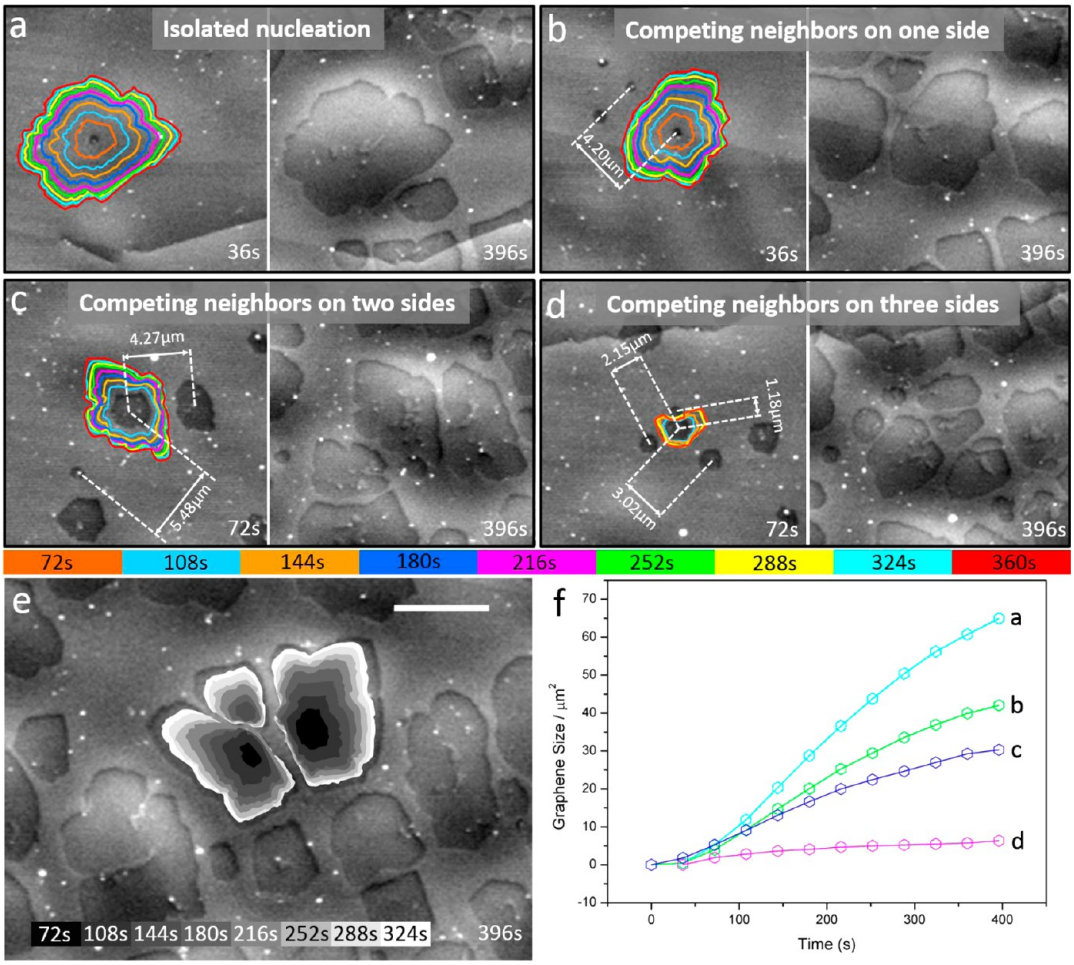

Figure 5. (a–d) Shape evolution of growing graphene sheets as a function of the local surrounding. The outlines of growing sheets are color coded according to the growth time provided in the color legend. Surface diffusion and growth competition within the capture layer influence growth shape and rate as shown in (e) and (f). Scale bar in (e) measures 5 μm.

exposed Cu due to sublimation is substantial[39] and more pronounced than under elevated pressures. However, imaging of the surface during growth demonstrates that the growing graphene sheets provide a barrier against sublimation.

As a consequence, the lateral expansion of the growing sheets leads to the formation of graphene-covered hills with valleys of uncovered copper in between them (see Figure 2, Figure SI 2, SI Movies M2, M4, and M5). The observed grain-dependent degree of hill-and-valley formation demonstrates that the sublimation rate is related to the crystallographic orientation of a grain (Figure 6a–d). As confirmed by EBSD measurements shown in Figure 6e and f, the hill-and-valley aspect is more pronounced and characteristic for graphene growth on ⟨100⟩- and ⟨110⟩-oriented grains, while relatively flat graphene sheets are formed on ⟨111⟩ grains. The extent of hill and valley formation furthermore depends on growth conditions. It increases with increasing growth time and is therefore more pronounced at low hydrocarbon flow rates. In the case of growth below 1000 °C, the effects of sublimation are far less pronounced (see Figure SI 6). For our growth conditions (4.4×10^{-2} Pa, 1000 °C, and 800 s of growth time), concave hills reached heights of up to 1.5 μm at a lateral expansion of a few 100 μm^2 for ⟨110⟩ and ⟨100⟩ grains.

Besides the effects of sublimation, the *in situ* observations also reveal a premelted and highly dynamic copper surface under conditions of LP-CVD at temperatures above 900 °C. The existence of a premelted surface layer on copper at this temperature is in agreement with the literature, according to which the first signs of surface premelting on copper can be detected at around 800 °C.[37,38] In fact, the premelting at the surface can be viewed as a wetting of the solid–vapor interface by its own liquid as the temperature approaches the melting point.[50] This quasi liquid exhibits structural, dynamic, and transport properties that are intermediate between those of the solid and liquid,[51] and it is affected by the underlying solid substrate. The degree and onset of premelting follows the order in the packing density; that is, the most open ⟨110⟩ face disorders at the lowest temperature, followed by the ⟨100⟩, while the ⟨111⟩ is more stable and shows weak premelting effects until the bulk

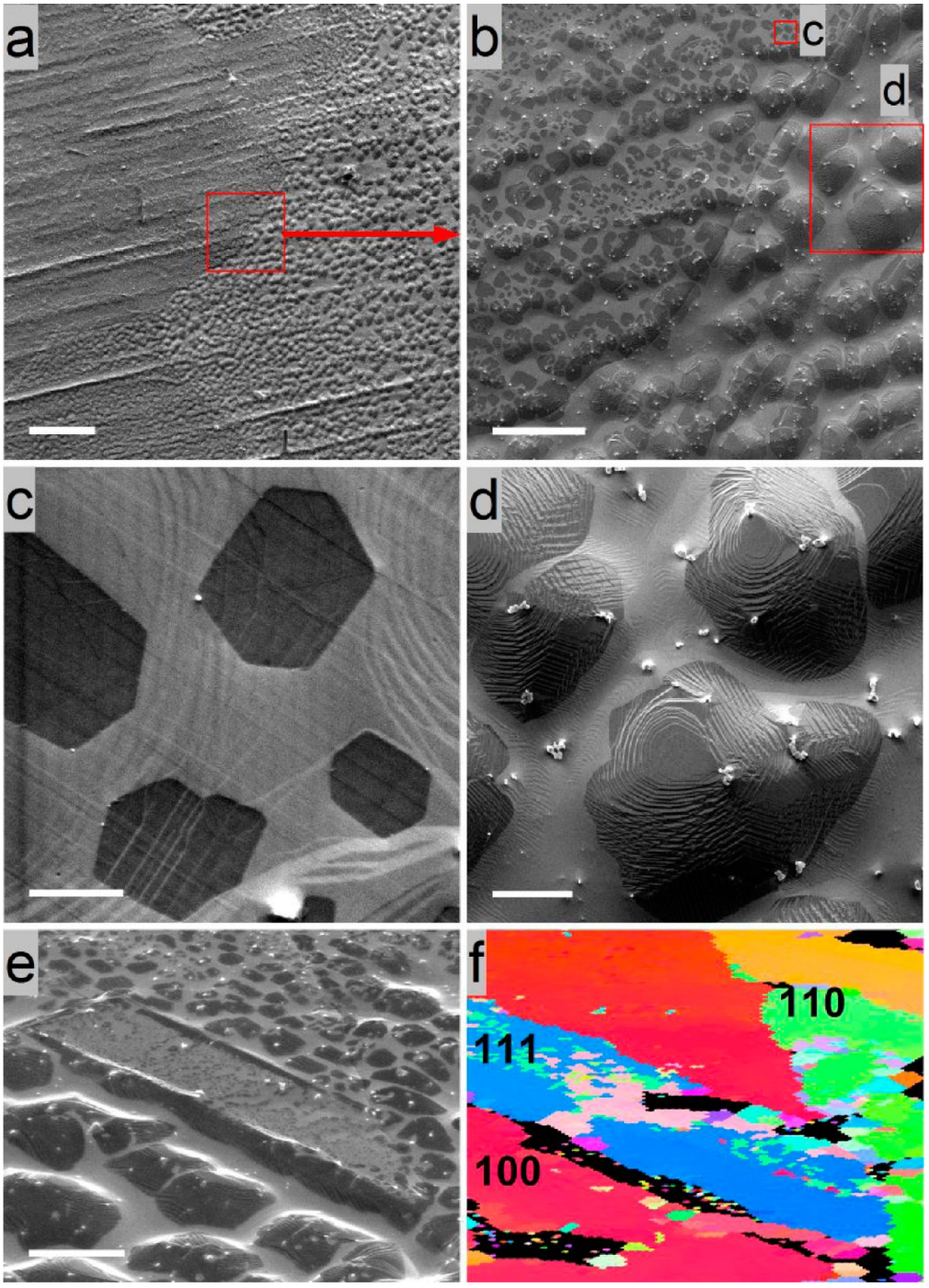

Figure 6. (a–d) Postgrowth SEM images showing relatively flat or convex-shaped graphene-coated regions. (a) and (b) show overview images; (c) and (d) representative details of the morphology on the respective grains. The EBSD map recorded from a region in (e) is shown in (f). Image (e) was recorded at a tilting angle of 70° as required for the EBSD measurement. Scale bars in (a) to (e) measure respectively 200, 20, 1, 5, and 10 μm.

melting temperature.[52] This is reflected in the different nucleation density observed for the ⟨111⟩ *versus* the other low-index surfaces: In agreement with I. Vlassiouk *et al.*,[39] we observe a higher nucleation density on the ⟨111⟩ compared to the ⟨100⟩ and ⟨110⟩ faces (see Figure 6a,b,e). It is a consequence of the higher degree of surface melting on the ⟨100⟩ and ⟨110⟩ surfaces, which causes a smoothening of the surface. Due to the absence of steps and edges, the number of nucleation sites is reduced as compared to the more stable ⟨111⟩-oriented surfaces. At lower temperatures, in the absence of surface premelting, we observe a similar nucleation density on ⟨110⟩, ⟨100⟩, and ⟨111⟩ grains (see Figure SI 7). Besides premelting, sublimation might also play a role in grain-orientation-dependent nucleation and growth, as it influences

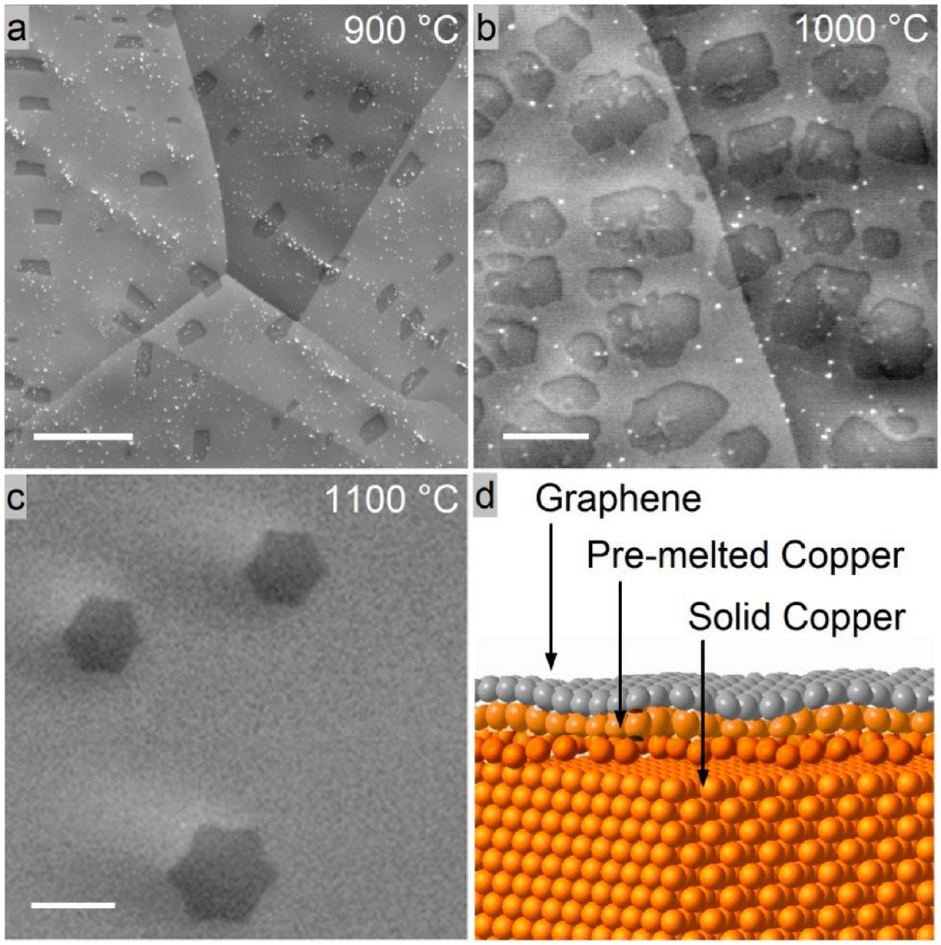

Figure 7. *In situ* **images recorded during growth at different temperature. With increasing temperature, the surface processes start to decouple from the crystalline order in the bulk of the grain due to increased thickness of the surface melt layer. (a) Growing sheets at 900 °C show a grain-orientation-dependent shape and orientation alignment. (b) No clear shape and orientation relation is detected in the case of growth at 1000 °C. (c) Above the melting point, hexagon-shaped graphene sheets grow locally in concordance. (d) Schematic picture of graphene on a surface premelted Cu layer. The scale bars measure 10, 5, and 1 μm in (a), (b), and (c), respectively.**

the lifetime and diffusion of growth species on the surface.[30]

Due to surface premelting, the actual graphene growth can be decoupled from the crystalline order in the bulk. Under LP-CVD conditions on polycrystalline Cu it is therefore possible to simultaneously observe graphene sheets that grow with or without evident orientation alignment on differently oriented grains.[36,43] For growth at 900 °C, grain-orientation-dependent graphene shapes[36] and orientation alignment of grown sheets are dominant[39] (see Figure 7a). With increasing temperature, the wetting layer thickens and processes on the surface start to decouple from the atomic arrangement in the underlying grain. At 1000 °C, growth proceeds largely decoupled from the bulk crystalline order and neither evident alignment of growth directions nor grain-dependent shapes are observed for most of the grains (Figure 7b). At this temperature, the migration of grain boundaries below growing sheets does not lead to significant disturbance in the growth behavior (Figure SI 8 and SI Movie M2). Only some shapes of hexagonal symmetry are observed, which is due to growth on Cu ⟨111⟩ grains with a higher stability against premelting and better lattice matching[53] (see Figures 2 and 6c).

Finally, at and above the Cu melting point, in the absence of crystalline order, graphene grows in hexagonal shapes, as can be seen in Figure 7c. Growth of graphene on liquid copper was first demonstrated by Geng *et al.*,[54] who found perfectly hexagon-shaped graphene flakes. As can be seen in Figure 7c, local orientation alignment can even be observed on liquid copper. This could be indicative for the existence of a close-packed structural ordering within the surface layer of the copper melt.[55] It is important to mention here that the atmosphere in the chamber has an influence on the surface mobility. Indeed, we have observed that hydrogen increases the mobility of the copper surface, confirming the findings of Sidorenko *et al.*[56]

In summary, the existence of a surface premelted layer has several implications: First, it leads to a partial decoupling of the growth from the copper atomic

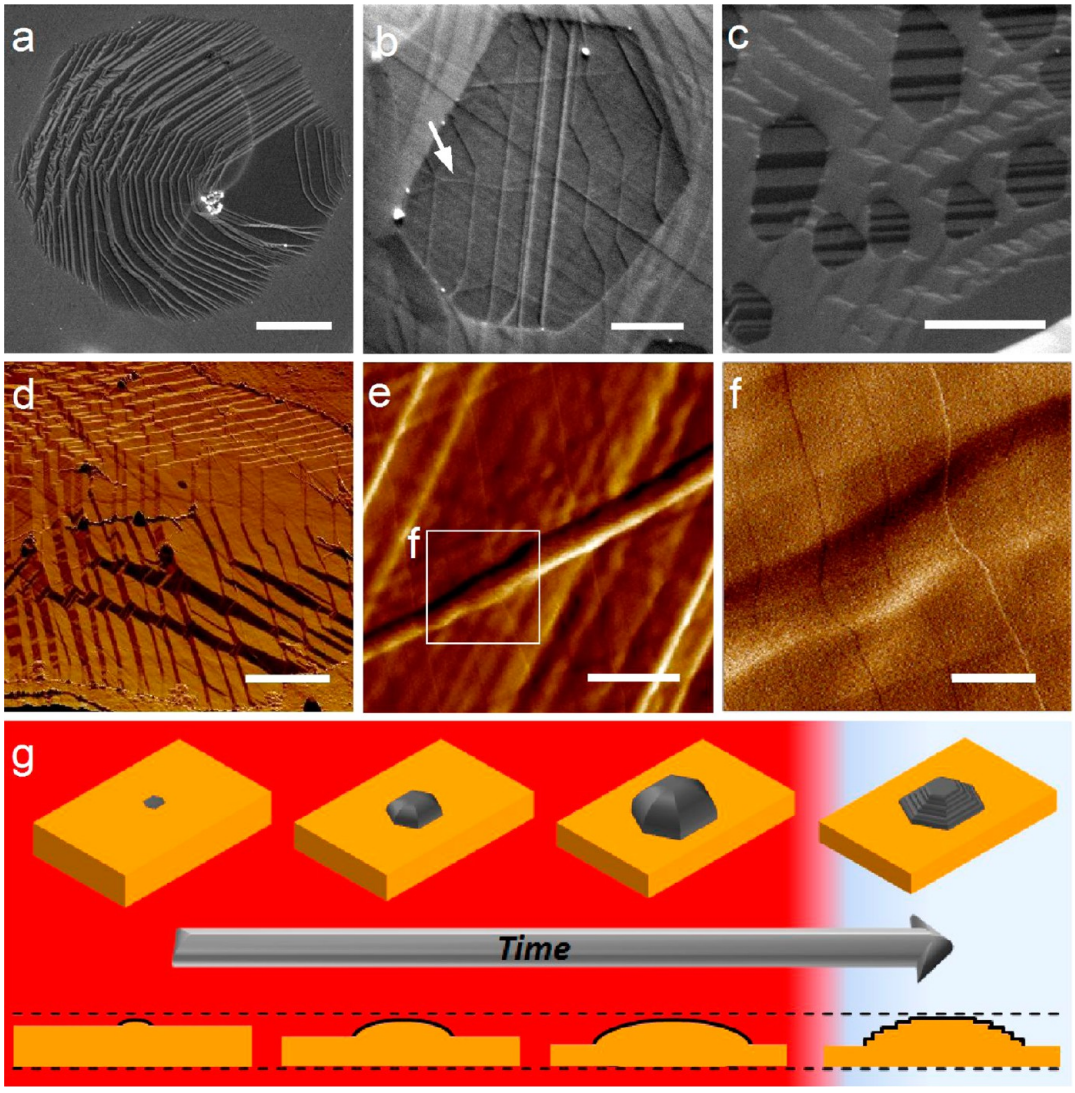

Figure 8. Postgrowth SEM (a–c) and AFM (d–f) images recorded after growth show graphene-induced copper surface reconstruction. In (e) and (f) details of a graphene wrinkle (similar to the one marked with an arrow in (b)) with particular stripes are shown. Note that the copper surface reconstruction is continuous across the wrinkle. (g) Schematic illustration showing the sublimation-induced hill and valley formation during graphene growth and subsequent surface faceting during cooling. Scale bars measure 2 μm (a), 500 nm (b), 1 μm (c), 10 μm (d), 100 nm (e), and 20 nm (f).

arrangement in the bulk even below the copper melting point (see schematic drawing in Figure 7d). Second, it provides locally an atomically flat and electronically homogeneous support for allowing carbon atoms to assemble and self-organize with a minimum of interference from the support. Furthermore, due to the absence of steps and kinks, the nucleation density on premelted copper is strongly reduced as compared to low-temperature growth.

Surface Reconstruction during Cooling. The ESEM reveals that the covering graphene layer induces a distinct recrystallization of the surface melted layer during cooling, which can lead to preferential exposure of specific planes. This is evidenced by the appearance of crystallographically identical facets underneath different graphene sheets within single copper grains such as shown in Figure 8a,b and, particularly, in 8c. Similar grain-dependent surface step bunches have been observed by Kim *et al.*,[57] who attributed their formation to strain relaxation between graphene and the Cu lattice. Due to the low temperature at which the reconstruction takes place, the crystallization proceeds such that the overall surface morphology of graphene-covered areas is preserved. In the case of graphene-covered hills, the shape is therefore approximated through the formation of low-energy graphene–copper interfaces and step bunches.[57] Accordingly, different reconstructions are observed on differently oriented grains (see Figure 8). However, the copper surface reconstruction does not change the orientation of the already grown graphene lattice. This explains why Rasool *et al.*[58] found that different facets, steps, and edges of the copper substrate are overgrown with a perfect graphene honeycomb lattice.

Surface reconstruction during cooling has so far not been observed directly; however, it has been postulated on the basis of postgrowth observations.[59] Because the reconstruction happens after growth, it can give rise to confusions regarding the relation between graphene and the atomic arrangement at the surface of the substrate during growth.[58,60]

At higher spatial resolution, AFM reveals particular reconstructions in the form of regular steps, as shown in Figure 8f. These stripes are in agreement with graphene-induced Cu surface reconstructions observed by Wilson and Tian *et al.*[61,62] using STM, who, similarly to Kim *et al.*,[57] attributed the formation of regular stripes under graphene to strain release at the copper surface. As can be seen in Figure 8f, such stripes are continuous even across graphene wrinkles, indicating a strong coupling between the copper and graphene (Figure 8e,f). The existence of a strong coupling between copper and graphene is in agreement with the findings of Kidambi *et al.*[25] Using *in situ* XPS, they provided evidence for a temperature- and atmosphere-dependent coupling between film and substrate, which could play a role in the observed surface reconstructions.

However, particular surface reconstructions could also be indicative for the presence of small amounts of adsorbed oxygen.[63,64] Under conditions of graphene growth in the ESEM, the presence of small amounts of oxygen in the gas phase is confirmed by the MS. The presence of submonolayer amounts of oxygen that is dissolved in the surface melt could in fact be a requisite for the catalytic decomposition of the ethylene, especially,in the case of growth on liquid copper, where the typical high-energy sites, such as step edges and defects, are absent. Indeed, the active catalyst in CVD graphene growth on copper could have similarities to the case of catalytic methanol oxidation on copper: From *in situ* X-ray absorption studies it is known that the active copper phase contains small amounts of dissolved oxygen.[65,66] A possible role of oxygen in the catalytic decomposition of the hydrocarbon on copper is suggested by the successful growth of graphene under conditions of oxidative dehydrogenation.[67] Furthermore, it has been shown that oxygen has an influence on the sticking coefficients and the rate of hydrocarbon precursor decomposition on copper.[68−70]

According to the Cu−O phase diagram, a transition from stable Cu to Cu_2O can occur at oxygen partial pressures in the range of 10^{-3} Pa at around 830 °C.[71] For lower partial pressures, thermal faceting due to surface oxide formation is observed at lower temperature.[72] The structural changes induced by oxygen adsorption depend on the oxygen coverage and initial crystallography of the faces.[64,73,74]

Indeed, our TEM cross-section investigation of samples investigated after growth in the ESEM confirms the presence of a thin Cu_2O layer on the surface of the copper (see Figure SI 9).

Considering the many different CVD setups and growth conditions and the published variety of graphene shapes, it can be assumed that the leak tightness and oxygen partial pressure in the atmosphere during growth are important variable influencing the outcome. Although the role of oxygen in ambient and low-pressure CVD graphene growth has been discussed in the literature,[13,68] it is clear that its involvement in the catalytic decomposition and the surface chemistry of copper during growth and cooling needs further investigation.

CONCLUSION

This work demonstrates the unique potential of an *in situ* technique that enables simultaneous and direct observation of the active catalyst and the forming product. Low-pressure CVD growth of graphene inside the chamber of an environmental SEM reveals the dynamic nature of the copper substrate and demonstrates that growth at high temperature occurs on a premelted, highly mobile copper surface. Surface dynamics are strongly dependent on the copper grain orientation, temperature, and atmosphere and have to be taken into account in the modeling of graphene formation. Real-time observation of graphene nucleation and growth provides relevant insight into the growth mechanism under LP-CVD. It is confirmed that nucleation starts after an induction period during which the surface saturates in growth species. From the growth behavior, three growth phases can be abstracted. In the first phase, a depletion zone is built up at the growth front. Once the depletion zone has fully developed, the growth mode changes from attachment- to diffusion-limited, and the second growth phase starts. During this phase, the presence of a capturing/diffusion zone at growth fronts is evidenced by the observed mutual influence of neighboring sheets. Once capturing/diffusion zones of neighboring sheets overlap, the third phase is reached. Growth at the corresponding growth fronts diminishes until a balance is reached between graphene etching and growth. The contributions of the described phases to the overall growth process certainly depend on the type of hydrocarbon source, the atmosphere pressure, and hydrocarbon/hydrogen ratio and should be systematically investigated. However, the ESEM study demonstrates that a correct growth model can be built only on the basis of direct observation of growing sheets and that an integrating analysis of the graphene-covered area after growth is insufficient.

In situ growth in the ESEM furthermore demonstrates that the relation between graphene and the copper surface during growth is different from the one observed after cooling in postgrowth characterization.[34] This is an important finding that has to be taken into account in the discussion of the influence of the substrate on the graphene growth,[15,16,40] specifically

concerning preferential alignment,[20] growth across grain boundaries,[19] and the many different nuclei shapes reported on different facets.[8]

The observed surface reconstruction during cooling suggests the presence of small amounts of oxygen that are dispersed as an impurity in the surface melted layer and could convert the Cu metal into a potent catalyst for hydrocarbon dissociation. Further studies will be required to elucidate the role of residual oxygen in CVD growth, and it is strongly suggested that the oxygen concentration is monitored and reported in future growth studies.

In situ ESEM will certainly play an important role in future graphene 2D material research because imaging of atomic thin sheets on a metal catalyst inside a microscope at variable magnification and temperatures under relevant conditions enables kinetic and mechanistic studies in a novel and unparalleled way.

Finally, this report demonstrates the high sensitivity of the secondary electron signal to morphological changes at the surface and the presence of atomically thin layers of carbon and, furthermore, the instruments' capability in terms of *in situ* surface science experiments.

METHODS

***In Situ* CVD Growth.** *In situ* CVD growth experiments were performed inside the chamber of a commercial ESEM (FEI Quantum 200). The instrument is equipped with a heating stage (FEI), a gas supply unit (mass flow controllers from Bronkhorst), and a mass spectrometer (Pfeiffer OmniStar) for the analysis of the chamber atmosphere. The vacuum system of the ESEM was upgraded with oil-free prevacuum pumps. Polycrystalline copper foils from Alfa Aesar were used as substrate (99.999% purity). Prior to all CVD growth experiments, the chamber of the ESEM was plasma cleaned. All samples were annealed at 1000 °C under a hydrogen flow of 8 sccm at a pressure of around 4.4×10^{-2} Pa for 50 min inside the chamber. The temperature was measured *via* a K-type thermocouple that was spot-welded onto the substrate. CVD growth was performed at 1000 °C using a flow of 4 sccm H_2 and 0.1 sccm of C_2H_4 at a total chamber pressure of $(2-4) \times 10^{-2}$ Pa. During the experiments, the microscope was operated at an acceleration voltage of 5.0 kV. Images were recorded using the secondary electron signal collected by a standard Everhart Thornley detector (ETD) during sample annealing, CVD growth, and cooling. The scan rate was set to one image per 36 s for M1, M2, and M3, respectively. ESEM movies are shown at 7 (M1) and 3 (M2) frames per second. No influence of the electron beam on the growth process could be observed. The imaged regions and their respective surroundings showed similar behavior, as evidenced by changing the magnification or by moving the sample under the beam. Furthermore, no electron-beam-induced contamination was observed at elevated temperatures.

Raman. Raman spectroscopy measurements were performed using a Horiba/Jobin-Yvon T64000 spectrometer (Villeneuve D'Ascq, France) with a Coherent Innova 400 (Santa Clara, CA, USA) argon-ion laser operating at 514.5 nm for the excitation. The Raman data were collected with a multichannel CCD detector. A laser power of 20 mW at the sample and an objective with a 100× magnification were used. The confocal approach has been adopted to reduce the background scattering with respect to the graphene signal. To obtain a satisfactory signal-to-noise ratio, the spectra were recorded with integration times of 60 s, in total number of 10 accumulations.

EBSD. The EBSD patterns were acquired using the EDAX Digiview detector installed on a SEM FEI NovaNanoSEM 230. Analysis of EBSD patterns, including phase identification and generation of orientation maps, was performed with the EDAX OMI 5.31 program.

AFM. Images were taken on a Bruker Sharp Nitride Lever probe (SNL-10). Imaging was done in tapping mode using a V-shaped cantilever probe B (silicon-tip on Nitride Lever with frequency $f_0 = 40-75$ kHz and spring constant $k = 0.32$ N m).

STM. Measurements were conducted using a commercial Bruker STM (multimode 8) under ambient pressure at room temperature. A bias voltage of 6 mV was applied at a tunneling current of 3.5 nA. A mechanically cut Pt−Ir tip was used.

TEM. HRTEM image of graphene−copper was taken by a FEI aberration-corrected Titan 80-300 TEM operated at 300 kV.

Conflict of Interest: The authors declare no competing financial interest.

Supporting Information Available: ESEM movies showing the copper surface during annealing in hydrogen, the metal-catalyzed CVD growth of graphene on a copper surface at 1000 °C, and copper surface reconstruction during cooling. AFM movies recorded after growth. EDX characterization of silica particles. Raman and STM characterization of the grown graphene. Supporting figures. This material is available free of charge *via* the Internet at http://pubs.acs.org.

Acknowledgment. Z.-J.W. is grateful to the CSC (Chinese Scholarship Council) for financing his Ph.D. at the FHI. The authors acknowledge S. Hofmann, P. Kidambi, and Rob Weatherup from the University of Cambridge, UK, for helpful discussions. M. Albrecht from the Leibniz-Institut für Kristallzüchtung in Berlin is acknowledged for EBSD measurements. Z.-J.W., G.W., and M.-G.W. modified the ESEM and performed all *in situ* ESEM as well as TEM and AFM experiments and analyzed the data. T.L., A.K.-H., M.K., M.P., Q.L., and L.C. were involved in the postgrowth characterization. M.-G.W. and Z.-J.W. wrote the manuscript. R.S. provided scientific guidance.

REFERENCES AND NOTES

1. Bae, S.; Kim, H.; Lee, Y.; Xu, X. F.; Park, J. S.; Zheng, Y.; Balakrishnan, J.; Lei, T.; Kim, H. R.; Song, Y. I.; *et al.* Roll-to-Roll Production of 30-inch Graphene Films for Transparent Electrodes. *Nat. Nanotechnol.* **2010**, *5*, 574–578.
2. Li, X. S.; Cai, W. W.; An, J. H.; Kim, S.; Nah, J.; Yang, D. X.; Piner, R.; Velamakanni, A.; Jung, I.; Tutuc, E.; *et al.* Large-Area Synthesis of High-Quality and Uniform Graphene Films on Copper Foils. *Science* **2009**, *324*, 1312–1314.
3. Sutter, P. Epitaxial Graphene: How Silicon Leaves the Scene. *Nat. Mater.* **2009**, *8*, 171–172.
4. Eswaraiah, V.; Aravind, S. S. J.; Ramaprabhu, S. Top Down Method for Synthesis of Highly Conducting Graphene by Exfoliation of Graphite Oxide using Focused Solar Radiation. *J. Mater. Chem.* **2011**, *21*, 6800–6803.
5. Amini, S.; Garay, J.; Liu, G.; Balandin, A. A.; Abbaschian, R. Growth of Large-Area Graphene Films from Metal-Carbon Melts. *J. Appl. Phys.* **2010**, *108*, 094321–094328.
6. Choucair, M.; Thordarson, P.; Stride, J. A. Gram-Scale Production of Graphene Based on Solvothermal Synthesis and Sonication. *Nat. Nanotechnol.* **2009**, *4*, 30–33.
7. Hernandez, Y.; Nicolosi, V.; Lotya, M.; Blighe, F. M.; Sun, Z. Y.; De, S.; McGovern, I. T.; Holland, B.; Byrne, M.; Gun'ko, Y. K.; *et al.* High-Yield Production of Graphene by Liquid-Phase Exfoliation of Graphite. *Nat. Nanotechnol.* **2008**, *3*, 563–568.
8. Jacobberger, R. M.; Arnold, M. S. Graphene Growth Dynamics on Epitaxial Copper Thin Films. *Chem. Mater.* **2013**, *25*, 871–877.
9. Vlassiouk, I.; Regmi, M.; Fulvio, P. F.; Dai, S.; Datskos, P.; Eres, G.; Smirnov, S. Role of Hydrogen in Chemical Vapor

Deposition Growth of Large Single- Crystal Graphene. *ACS Nano* **2011**, *5*, 6069–6076.
10. Wu, B.; Geng, D. C.; Guo, Y. L.; Huang, L. P.; Xue, Y. Z.; Zheng, J.; Chen, J. Y.; Yu, G.; Liu, Y. Q.; Jiang, L.; *et al*. Equiangular Hexagon-Shape-Controlled Synthesis of Graphene on Copper Surface. *Adv. Mater.* **2011**, *23*, 3522–3525.
11. Zhang, Y.; Zhang, L.; Kim, P.; Ge, M.; Li, Z.; Zhou, C. Vapor Trapping Growth of Single-Crystalline Graphene Flowers: Synthesis, Morphology, and Electronic Properties. *Nano Lett.* **2012**, *12*, 2810–2816.
12. Li, X. S.; Magnuson, C. W.; Venugopal, A.; Tromp, R. M.; Hannon, J. B.; Vogel, E. M.; Colombo, L.; Ruoff, R. S. Large-Area Graphene Single Crystals Grown by Low-Pressure Chemical Vapor Deposition of Methane on Copper. *J. Am. Chem. Soc.* **2011**, *133*, 2816–2819.
13. Hao, Y. F.; Bharathi, M. S.; Wang, L.; Liu, Y. Y.; Chen, H.; Nie, S.; Wang, X. H.; Chou, H.; Tan, C.; Fallahazad, B.; *et al*. The Role of Surface Oxygen in the Growth of Large Single-Crystal Graphene on Copper. *Science* **2013**, *342*, 720–723.
14. Piccinin, S.; Zafeiratos, S.; Stampfl, C.; Hansen, T. W.; Havecker, M.; Teschner, D.; Bukhtiyarov, V. I.; Girgsdies, F.; Knop-Gericke, A.; Schlogl, R.; *et al*. Alloy Catalyst in a Reactive Environment: The Example of Ag-Cu Particles for Ethylene Epoxidation. *Phys. Rev. Lett.* **2010**, *104*, 035503.
15. Kandemir, T.; Girgsdies, F.; Hansen, T. C.; Liss, K. D.; Kasatkin, I.; Kunkes, E. L.; Wowsnick, G.; Jacobsen, N.; Schlogl, R.; Behrens, M. *In-Situ* Study of Catalytic Processes: Neutron Diffraction of a Methanol Synthesis Catalyst at Industrially Relevant Pressure. *Angew. Chem., Int. Ed.* **2013**, *52*, 5166–5170.
16. Behrens, M.; Studt, F.; Kasatkin, I.; Kuhl, S.; Havecker, M.; Abild-Pedersen, F.; Zander, S.; Girgsdies, F.; Kurr, P.; Kniep, B. L. The Active Site of Methanol Synthesis over Cu/ZnO/Al_2O_3 Industrial Catalysts. *Science* **2012**, *336*, 893–897.
17. Sutter, P.; Flege, J.; Sutter, E. Epitaxial Graphene on Ruthenium. *Nat. Mater.* **2008**, *7*, 406–411.
18. Loginova, E.; Bartelt, N. C.; Feibelman, P. J.; McCarty, K. F. Evidence for Graphene Growth by C Cluster Attachment. *New J. Phys.* **2008**, *10*, 093026.
19. Loginova, E.; Bartelt, N. C.; Feibelman, P. J.; McCarty, K. F. Factors Influencing Graphene Growth on Metal Surfaces. *New J. Phys.* **2009**, *11*, 063046.
20. Odahara, G.; Otani, S.; Oshima, C.; Suzuki, M.; Yasue, T.; Koshikawa, T. *In-Situ* Observation of Graphene Growth on Ni(111). *Surf. Sci.* **2011**, *605*, 1095–1098.
21. Cui, Y.; Fu, Q.; Zhang, H.; Tan, D.; Bao, X. Dynamic Characterization of Graphene Growth and Etching by Oxygen on Ru(0001) by Photoemission Electron Microscopy. *J. Phys. Chem. C* **2009**, *113*, 20365–20370.
22. Günther, S.; Dänhardt, S.; Wang, B.; Bocquet, M.-L.; Schmitt, S.; Wintterlin, J. Single Terrace Growth of Graphene on a Metal Surface. *Nano Lett.* **2011**, *11*, 1895–1900.
23. Dong, G. C.; Baarle, D. W.; Rost, M. J.; Frenken, J. W. M. Graphene Formation on Metal Surfaces Investigated by *in-Situ* Scanning Tunneling Microscopy. *New J. Phys.* **2012**, *14*, 053033.
24. Patera, L.; Patera, L. L.; Africh, C.; Weatherup, R. S.; Blume, R.; Bhardwaj, S.; Castellarin-Cudia, C.; Knop-Gericke, A.; Schloegl, R.; Comelli, G.; Hofmann, S.; *et al*. In Situ Observations of the Atomistic Mechanisms of Ni Catalyzed Low Temperature Graphene Growth. *ACS Nano* **2013**, *7*, 7901–7912.
25. Kidambi, P. R.; Bayer, B. C.; Blume, R.; Wang, Z. J.; Baehtz, C.; Weatherup, R. S.; Willinger, M. G.; Schloegl, R.; Hofmann, S. Observing Graphene Grow: Catalyst–Graphene Interactions during Scalable Graphene Growth on Polycrystalline Copper. *Nano Lett.* **2013**, *13*, 4769–4778.
26. Wofford, J. M.; Nie, S.; McCarty, K. F.; Bartelt, N. C.; Dubon, O. D. Graphene Islands on Cu Foils: The Interplay between Shape, Orientation, and Defects. *Nano Lett.* **2010**, *10*, 4890–4896.
27. Nie, S.; Wofford, J. M.; Bartelt, N. C.; Dubon, O. D.; McCarty, K. F. Origin of the Mosaicity in Graphene Grown on Cu(111). *Phys. Rev. B* **2011**, *84*, 155425.
28. Takahashi, K.; Yamada, K.; Kato, H.; Hibino, H.; Homma, Y. *In Situ* Scanning Electron Microscopy of Graphene Growth on Polycrystalline Ni Substrate. *Surf. Sci.* **2012**, *606*, 728–732.
29. Kim, H.; Mattevi, C.; Calvo, M. R.; Oberg, J. C.; Artiglia, L.; Agnoli, S.; Hirjibehedin, C. F.; Chhowalla, M.; Saiz, E. Activation Energy Paths for Graphene Nucleation and Growth on Cu. *ACS Nano* **2012**, *6*, 3614–3623.
30. Celebi, K.; Cole, M. T.; Choi, J. W.; Wyczisk, F.; Legagneux, P.; Rupesinghe, N.; Robertson, J.; Teo, K. B. K.; Park, H. G. Evolutionary Kinetics of Graphene Formation on Copper. *Nano Lett.* **2013**, *13*, 967–974.
31. Seiler, H. Secondary Electron Emission in the Scanning Electron Microscope. *J. Appl. Phys.* **1983**, *54*, R1–R18.
32. Gartland, P. O.; Berge, S.; Slagsvold, B. J. Photoelectric Work Function of a Copper Single Crystal for the (100), (110), (111), and (112) Faces. *Phys. Rev. Lett.* **1972**, *28*, 738–739.
33. Kochat, V.; Pal, A. N.; Sneha, E. S.; Sampathkumar, A.; Gairola, A.; Shivashankar, S. A.; Raghavan, S.; Ghosh, A. High Contrast Imaging and Thickness Determination of Graphene with in-Column Secondary Electron Microscopy. *J. Appl. Phys.* **2011**, *110*, 014315.
34. Robinson, Z. R.; Tyagi, P.; Murray, T. M.; Ventrice, C. A., Jr. Substrate Grain Size and Orientation of Cu and Cu–Ni Foils used for the Growth of Graphene Films. *J. Vac. Sci. Technol.* **2012**, *30*, 011401.
35. Wood, J. D.; Schmucker, S. W.; Lyons, A. S.; Pop, E.; Lyding, J. W. Effects of Polycrystalline Cu Substrate on Graphene Growth by Chemical Vapor Deposition. *Nano Lett.* **2011**, *11*, 4547–4554.
36. Murdock, A. T.; Koos, A.; Ben Britton, T.; Houben, L.; Batten, T.; Zhang, T.; Wilkinson, A. J.; Dunin-Borkowski, R. E.; Lekka, C. E.; Grobert, N. Controlling the Orientation, Edge Geometry, and Thickness of Chemical Vapor Deposition Graphene. *ACS Nano* **2013**, *7*, 1351–1359.
37. Frenken, J. W. M.; Van der Veen, J. F. Observation of Surface Melting. *Phys. Rev. Lett.* **1985**, *54*, 134–137.
38. Chatterjee, B. Anisotropy of Melting for Cubic Metals. *Nature* **1978**, *275*, 203.
39. Vlassiouk, I.; Smirnov, S.; Regmi, M.; Surwade, S. P.; Srivastava, N.; Feenstra, R.; Eres, G.; Parish, C.; Lavrik, N.; Datskos, P.; *et al*. Graphene Nucleation Density on Copper: Fundamental Role of Background Pressure. *J. Phys. Chem. C* **2013**, *117*, 18919–18926.
40. Ferrari, A. C.; Meyer, J. C.; Scardaci, V.; Casiraghi, C.; Lazzeri, M.; Mauri, F.; Piscanec, S.; Jiang, D.; Novoselov, K. S.; Roth, S.; *et al*. Raman Spectrum of Graphene and Graphene Layers. *Phys. Rev. Lett.* **2006**, *97*, 187401.
41. Graf, D.; Molitor, F.; Ensslin, K.; Stampfer, C.; Jungen, A.; Hierold, C.; Wirtz, L. Spatially Resolved Raman Spectroscopy of Single- and Few-Layer Graphene. *Nano Lett.* **2007**, *7*, 238–242.
42. Rasool, H. I.; Song, E. B.; Mecklenburg, M.; Regan, B. C.; Wang, K. L.; Weiller, B. H.; Gimzewski, J. K. Atomic-Scale Characterization of Graphene Grown on Copper (100) Single Crystals. *J. Am. Chem. Soc.* **2011**, *133*, 12536–12543.
43. Luo, Z.; Kim, S.; Kawamoto, N.; Rappe, A. M.; Johnson, A. T. C. Growth Mechanism of Hexagonal-Shape Graphene Flakes with Zigzag Edges. *ACS Nano* **2011**, *5*, 9154–9160.
44. Artyukhov, V. I.; Liua, Y.; Yakobson, B. I. Equilibrium at the Edge and Atomistic Mechanisms of Graphene Growth. *PNAS* **2012**, *109*, 15136–15140.
45. Venables, J. A.; Spiller, D. T.; Hanbücken, M. Nucleation and Growth of Thin Films. *Rep. Prog. Phys.* **1984**, *47*, 399–459.
46. Reichelt, K. Nucleation and Growth of Thin Films. *Vacuum* **1988**, *38*, 1083–1099.
47. Meca, E.; Lowengrub, J.; Kim, H.; Mattevi, C.; Shenoy, V. B. Epitaxial Graphene Growth and Shape Dynamics on Copper: Phase-Field Modeling and Experiments. *Nano Lett.* **2013**, *13*, 5692–5697.
48. Eres, G.; Regmi, M.; Rouleau, C. M.; Chen, J. H.; Ivanov, I. N.; Puretzky, A. A.; Geohegare, D. B. Cooperative Island Growth of Large-Area Single-Crystal Graphene on Copper Using Chemical Vapor Deposition. *ACS Nano* **2014**, *8*, 5657–566.

49. Li, X. S.; Magnuson, C. W.; Venugopal, A.; An, J. H.; Suk, J. W.; Han, B. Y.; Borysiak, M.; Cai, W. W.; Velamakanni, A.; Zhu, Y. W. Graphene Films with Large Domain Size by a Two-Step Chemical Vapor Deposition Process. *Nano Lett.* **2010**, *10*, 4328–4334.
50. Mei, S. Q.; Lu, K. Melting and Superheating of Crystalline Solids: From Bulk to Nanocrystals. *Prog. Mater. Sci.* **2007**, *52*, 1175–1262.
51. Polčik, M.; Wilde, L.; Haase, J. Partial Order of the Quasiliquid During Surface Melting of Al (110). *Phys. Rev. Lett.* **1997**, *78*, 491–494.
52. Häkkinen, H.; Manninen, M. Computer Simulation of Disordering and Premelting of Low-Index Faces of Copper. *Phys. Rev. B* **1992**, *46*, 1725–1742.
53. Gao, L.; Guest, J. R.; Guisinger, N. P. Epitaxial Graphene on Cu(111). *Nano Lett.* **2010**, *10*, 3512–3516.
54. Geng, D. C.; Wu, B.; Guo, Y. L.; Huang, L. P.; Xue, Y. Z.; Chen, J. Y.; Yu, G.; Jiang, L.; Hu, W. P.; Liu, Y. Q. Uniform Hexagonal Graphene Flakes and Films Grown on Liquid Copper Surface. *PNAS* **2012**, *109*, 7992–7996.
55. DiMasi, E.; Tostmann, H.; Shpyrko, O. G.; Deutsch, M.; Pershan, P. S.; Ocko, B. M. Surface-Induced Order in Liquid Metals and Binary Alloys. *J. Phys.: Condens. Matter* **2000**, *12*, A209–A214.
56. Sidorenko, V. M.; Sidorak, I. I. Boundary and Volume Diffusion of Hydrogen in Copper, Nickel, and Iron. *Mater. Sci.* **1973**, *9*, 372–375.
57. Kim, D. W.; Lee, J.; Kim, S. J.; Jeon, S.; Jung, H. T. The Effects of the Crystalline Orientation of Cu Comains on the Formation of Nanoripple Arrays in CVD-Grown Graphene on Cu. *J. Mater. Chem. C* **2013**, *1*, 7819–7824.
58. Rasool, H. I.; Song, E. B.; Allen, M. J.; Wassei, J. K.; Kaner, R. B.; Wang, K. L.; Weiller, B. H.; Gimzewski, J. K. Continuity of Graphene on Polycrystalline Copper. *Nano Lett.* **2011**, *11*, 251–256.
59. Paronyan, T. M.; Pigos, E. M.; Chen, G.; Harutyunyan, A. R. Formation of Ripples in Graphene as a Result of Interfacial Instabilities. *ACS Nano* **2011**, *5* (12), 9619–9627.
60. Mi, X.; Meunier, V.; Koratkar, N.; Shi, Y. Facet-Insensitive Graphene Growth on Copper. *Phys. Rev. B* **2012**, *85*, 155436.
61. Wilson, N. R.; Marsden, A. J.; Saghir, M.; Bromley, C. J.; Schaub, R.; Costantini, G.; White, T. W.; Partridge, C.; Barinov, A.; Dudin, P. Weak Mismatch Epitaxy and Structural Feedback in Graphene Growth on Copper Foil. *Nano. Res.* **2013**, *6*, 99–112.
62. Tian, J.; Cao, H.; Wu, W.; Yu, Q.; Guisinger, N. P.; Chen, Y. P. Graphene Induced Surface Reconstruction of Cu. *Nano Lett.* **2012**, *12*, 3893–3899.
63. Guillemot, L.; Bobrov, K. Morphological Instability of the Cu(110)−(2×1)−O Surface under Thermal Annealing. *Phys. Rev. B* **2011**, *83*, 075409.
64. Sotto, M. Oxygen Induced Reconstruction of (h11) and (100) Faces of Copper. *Surf. Sci.* **1992**, *260*, 235–244.
65. Böttger, I.; Schedel-Niedrig, T.; Timpe, O.; Gottschall, R.; Havecker, M.; Ressler, T.; Schlogl, R. Catalytic Methanol Oxidation over Copper: Observation of Reaction-Induced Nanoscale Restructuring by Means of in Situ Time-Resolved X-ray Absorption Spectroscopy. *Chem.—Eur. J.* **2000**, *6* (10), 1870–1876.
66. Schedel-Niedrig, T.; Neisius, T.; Bottger, N.; Kitzelmann, E.; Weinberg, G.; Demuth, D.; Schlogl, R. Copper (sub)Oxide Formation: A Surface Sensitive Characterization of Model Catalysts. *Phys. Chem. Chem. Phys.* **2000**, *2*, 2407–2417.
67. Bernard, L. S.; Spina, M.; Jacimovic, J.; Ribic, P. R.; Walter, A.; Oberli, D. Y.; Horvath, E.; Forro, L.; Magrez, A. Functionalized Graphene Grown by Oxidative Dehydrogenation Chemistry. *Carbon* **2014**, *71*, 11–19.
68. Robinson, Z. R.; Ong, E. W.; Mowll, T. R.; Tyagi, P.; Gaskill, D. K.; Geisler, H.; Ventrice, C. A. Influence of Chemisorbed Oxygen on the Growth of Graphene on Cu(100) by Chemical Vapor Deposition. *J. Phys. Chem. C* **2013**, *117*, 23919–23927.
69. Au, C. T.; Roberts, M. W. Photoelectron Spectroscopic Evidence for the Activation of Adsorbate Bonds by Chemisorbed Oxygen. *Chem. Phys. Lett.* **1980**, *74*, 472–474.
70. Alstrup, I.; Chorkendorff, I.; Ullmann, S. The Interaction of CH, at High Temperatures with Clean and Oxygen Precovered Cu(100). *Surf. Sci.* **1992**, *264*, 95–102.
71. Neumann, J. P.; Zhong, T.; Chang, Y. A. The Cu−O (Copper-Oxygen) System. *Bull. Alloy Phase Diagr.* **1984**, *5*, 136–140.
72. Reinecke, N.; Taglauer, E. The Kinetics of Oxygen-Induced Faceting of Cu (115) and Cu (119) Surfaces. *Surf. Sci.* **2000**, *454−456*, 94–100.
73. Simmons, G. W.; Mitchell, D. G.; Lawless, K. R. LEED and HEED Studies of the Interaction of Oxygen with Single Crystal Surfaces of Copper. *Surf. Sci.* **1967**, *8*, 130–164.
74. Boulliard, J. C.; Domange, J. L.; Sotto, M. Structural Changes of Vicinal Copper Surfaces Induced by Oxygen Adsorption. *Surf. Sci.* **1986**, *165*, 434–446.